Microstructure-property relationships in cement mortar with surface treatment of microbial induced carbonate precipitation

Lu Wang [a], Zhisheng Ren [a], Hao Wang [a], Xiao Liang [a], Shuhua Liu [a, *], Jun Ren [b], Yan He [c], Mingzhong Zhang [d]

[a] State Key Laboratory of Water Resources and Hydropower Engineering Science, Wuhan University, Wuhan, 430072, China

[b] School of Architecture and Planning, Yunnan University, Kunming, 650051, China

[c] School of Civil Engineering, Suzhou University of Science and Technology, Suzhou, 215011, China

[d] Department of Civil, Environmental and Geomatic Engineering, University College London, London, WC1E 6BT, UK

Abstract: Microbial induced calcite precipitation (MICP) can protect the surface of porous cement-based materials and enhance the durability of concrete, the efficiency of which depends on the near surface property. Therefore, this paper is aimed to investigate the effects of bacterial solution to cementation solution ratio (1:2, 1:1 and 2:1) and different calcium sources (calcium chloride, calcium nitrate and calcium acetate) on compressive strength and capillary water absorption coefficient of MICP-treated mortar and attempted to establish the relationship between microstructure and macroscopic property. The results indicated that the surface treatment by MICP significantly reduced the capillary water absorption coefficient, while it slightly affected the compressive strength of mortar. Supplying calcium source of calcium chloride or calcium nitrate, setting bacterial solution to cementation solution volume ratio of 1:1 were beneficial to improve the compressive strength and reduce the coefficient, in which the CH content of the near surface layer was reduced and the calcite content of that was increased, it showed limited influence on the hydration products of the interior substances. Nanoscale calcite generated in the near surface layer consumed the CH and filled in gel pores to increase the Ca/Si ratio of C–S–H. The increased compressive strength was due to the refined pore structure of the near surface layer, in which the combination effect of improved pore structure of the near surface layer and the precipitation layer of MICP on the surface effectively reduced the coefficients.

Keywords: Microbial induced calcite precipitation; Cement-based material; Surface treatment; Macroscopic property; Hydration products; Microstructure

1. Introduction

Cement-based materials are the most widely used construction materials due to their unique advantages such as superior mechanical property, easy to cast into different shapes, low production cost and better durability [1]. However, the concrete structures in service could be subject to atmospheric moisture (CO_2 or acid rain), water environments (soft water or sea water) or combined environment [2-4], as a result of which, the corrosion of steel reinforcement in structures would occur, leading to increased porosity and reduced mechanical properties [5,6]. The reactions of corrosive substances (e.g. CO_2) with the cement hydrates, e.g., $Ca(OH)_2$, can result in the decomposition of C–S–H gel and C-A-H [2-5]. This issue will become even worse in the presence of micro-cracks, in which the aggressive substances can ingress into concrete cover through surface cracks and thus deteriorate the concrete structures [7,8]. Therefore, the completeness of the surface mortar surface is crucial for maintaining the structures' performance and it is vital to improve the permeation resistance of the surface layers [9-11].

Currently, for surface treatment, different materials and approaches including the addition of water repellents or pore blockers and the protection of surface with coatings have been widely adopted to ensure the quality of concrete surface [12-14]. However, there still exist some disadvantages such as the different thermal expansion coefficients of the protective layer and the underlying layer, the degradation of the protective layer over time and the constant maintenance for the protective layer [15,16], which would hinder their widespread applications. To tackle these drawbacks and improve the efficiency of surface protection, a new technology based on microbial induced calcite precipitation (MICP) [12,17-19], has been applied in the surface protection of cement-based materials.

The early application of MICP technology has been attempted to the surface restoration of ancient buildings [14,20,21], in which the ancient clay roof tiles and tabia, the main surface materials, had been exposed to the environment for a long-term with a significant reduction of surface performance. The application of MICP technology was based on the brushing method for a soil sample or a tile, in which anti-corrosion characteristics and water resistance could be significantly improved [14,20]. Generally, the MICP technology exhibits a good compatibility with natural stones (marble and limestone) [22-26]. For instance, a dense biomineralized film in marble is formed through MICP technology with both immersion and brushing methods, which leads to an enhanced durability [27,28]. For limestone, the similar performances are observed for the specimens treated with the bacteria (Bacillus sphaericus LMG 225 57) under the optimal dosage of urea and calcium source, to that treated with ethylsilicates along with the decreased water absorption and resistance towards sonication [23,29]. Furthermore, the influence of pore structure on the protection effectiveness in limestone by MICP indicated that MICP technology can be effective and more feasible for macroporous stones than for microporous ones [11,24]. Moreover, surface treatment of

natural stone with MICP technology by spray method increased the surface coated mass and the formed calcite filling in the micro-cracks, which reduces the natural weathering actions on exposed stone [25]. Based on the visual observation, some spheroidal depositions on surface are formed using the immersion method of MICP on coquina core specimens, increasing the unit weight while decreasing the absorption [26,30].

Although it has been proved that the MICP technology has been successfully applied to improve surface property of ancient buildings and natural stones, its effects on the cement-based materials has been just explored. Some works had studied the effects of MICP technology with different surface treatment methods on surface mortar [6,31-34], such as immersion, spraying and immobilization brushing method. Under the MICP technology with immersion method, a protection layer was formed on the surface of cement-based materials and then improved its surface permeability resistance and resist the acid attack [6]. It has been reported that the protection effect of agar immobilization brushing method was better than that of immersion method and the thickness of the microbial precipitated coating layer on cement-based materials was about 10 μm [34,35]. Moreover, comparing with MICP technology, the immobilization brushing method was reported as the most effective methods in surface protection as it could reduce the capillary water absorption coefficient by 90% [36,37]. It is generally agreed that the surface treatment by MICP technology can generate a protection layer on the surface of the treated sample and reduce the capillary water absorption coefficient, leading to an improved durability. The protection effect of immobilization brushing method was better than that of immersion method, while the operational program of immobilization brushing method was more complex, which requires to the application of a simpler treatment. Moreover, in the perspective from microbiology, the effect of biomineralization on cementitious materials is highly dependent on the concentration of bacterial solution and cementation solution. However, the combined effects of bacterial solution to cementation solution volume ratio and different calcium sources in cementation solution on the protection effect of cement-based material have not been studied to date.

Therefore, an easier surface treatment method of MICP technology was proposed in this paper, and its reaction effect on macroscopic properties in relation to microstructure were investigated. Moreover, the combined effect of the ratio of bacterial solution-to-cementation solution and calcium source on surface treatment efficiency of cement-based materials by MICP technology was investigated as well, which is mainly focused on the relationship between microstructure and macroscopic properties. A series of tests were conducted to estimate the effects of bacterial solution-to-cementation solution volume ratios (1:2, 1:1 and 2:1) and calcium sources (calcium chloride, calcium nitrate and calcium acetate) on the properties of ordinary Portland cement mortar, including capillary water absorption coefficient, compressive strength, pore structure of near surface layer as

well as the mineral composition and morphology of mortar's surface and the near surface layer. Based on the obtained experimental data, the microstructure-property relationships in treated mortar was studied in a quantitative manner to gain insights into the underlying mechanisms.

2. Experimental program

2.1. Raw materials

Ordinary Portland cement P·O 42.5 and standard river sand according to GB175-2007 and GSB 08-1337-2018 respectively were used to prepare the mortar specimens in this study. The chemical composition of the cement is given in Table 1. The bacteria Sporosarcina pasteurii (CGMCC No. 1.3687) strain, a type of urea-hydrolysing and non-pathogenic bacterium provided by China General Microbiological Culture Collection Centre, was used in this study. The bacterial solution (BS) was stable bacterial solution cultured in laboratory with the absorbance of 1–1.2 and the urease activity of 30–35 mM urea/min. More details about the cultivation of stable bacterial solution can be found in references [38,39]. AR grade chemical reagents including pure calcium chloride (CC), calcium nitrate (CN), calcium acetate (CA) and urea were obtained from China National Pharmaceutical Group Corporation. The cementation solution (CS) was prepared by mixing the urea and calcium ions under the mole ratio of 1:1 and the concentration was controlled as 1 mol/L. Three types of cementation solutions (CS) were prepared as follows: CS1: a mixer of 1 mol/L urea with 1 mol/L CC (calcium chloride); CS2: a mixer of 1 mol/L urea with 1 mol/L CN (calcium nitrate); CS3: a mixer of 1 mol/L urea with 1 mol/L CA (calcium acetate).

Table 1 Chemical composition of ordinary Portland cement (wt.%).

CaO	SO_3	SiO_2	P_2O_5	Al_2O_3	Fe_2O_3	MgO	Na_2O	K_2O	TiO_2	CO_2	LOI
56.6	4.14	20.4	0.1	5.12	3.77	2.98	0.11	0.81	0.33	3.95	1.69

Note: LOI – loss on ignition.

2.2. Mix proportions and specimen preparation

The mortar specimens (40 mm × 40 mm × 40 mm) were prepared with water-to-cement (w/c) ratio of 0.5 and cement-to-sand (c/s) ratio of 1:3. The mix proportions of mortar cubes and the solutions used for the mortar surface treatment was presented in Table 2. The mixing and casting of mortar were conducted under an ambient condition (20 ± 2 °C, ≥50% RH). The specimens were demoulded after 24 h and then stored in a standard curing room (20 ± 1 °C, ≥90% RH) for 27 d. After that, they were put into a drying oven with 45 °C for 2 h to remove the water mark on the surface. For each specimen, to determine the increment in water penetration resistance, a sorptivity test, according to the RILEM 25 PEM (II-6) [12], was carried out. During the test, the top surface of each specimen was selected as the treated face, and then the four faces adjacent to the treated side were coated with epoxy resin, and a layer of aluminium adhesive was affixed to the four surfaces to ensure unidirectional absorption through the treated side, whereas the bottom surface was directly used without any treatment. A

schematic diagram of the surface treatment process is shown in Fig. 1. During the preparation, the layer of aluminium adhesive was affixed to the four surfaces above 1.5 cm of the treated side to form a container to contain bacterial solution and cementation solution. As seen in Table 2, different bacterial solution-to-cementation solution volume ratios and different cementation solutions would result in different effects on the surface properties and microstructure.

Table 2 Mix proportions of mortar cubes and the solutions used for surface treatment.

Mixture ID	Cement (g)	Sand (g)	Water (mL)	BS/CS volume ratio	BS (mL)	CS1 (mL)	CS2 (mL)	CS3 (mL)
M50	450	1350	225	-	-	-	-	-
M50A05				1:2	6	12	-	-
M50A10				1:1	9	9	-	-
M50A20				2:1	12	6	-	-
M50B05				1:2	6	-	12	-
M50B10				1:1	9	-	9	-
M50B20				2:1	12	-	6	-
M50C05				1:2	6	-	-	12
M50C10				1:1	9	-	-	9
M50C20				2:1	12	-	-	6

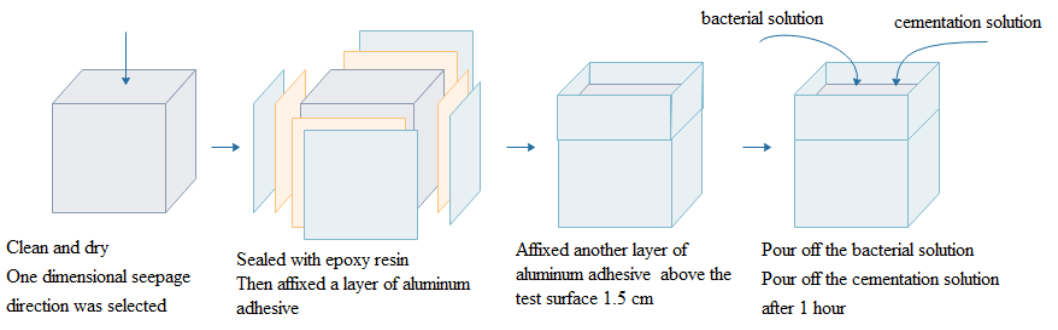

Fig. 1. Schematic illustration of the procedure of MICP surface treatment of mortar.

2.3. Test methods

2.3.1 Capillary water absorption test

After surface treatment, the extra aluminium adhesive above the treated surface was first peeled off. Then, all specimens were dried at 60 °C in a drying oven until differences on the mass loss ratio in 24 h was below 0.1%, and the ultimate mass was recorded. A holder was then put into a flat container and the treated mortars were then tested on the holder with testing face down, pouring water into the container slowly till the liquid level was 10 ± 1 mm above the bottom of the specimen. At designed time intervals (i.e., 0.5, 1, 2, 4, 8, 12, 24, 36 and 72 h), the specimens were weighted after drying the surface with a wet towel [12]. After weighing, the samples were immediately placed back into the water for curing. It should be noted that the test was conducted at a temperature of 20 °C and RH of about 60%. After the test, the water absorption per weight of the specimen was calculated using Eq.

(1) and the capillary water absorption coefficient k ($kg/m^2/h^{0.5}$) was determined as the slope of the regression line given the linear correlation using Eq. (2).

$$q = \frac{Q}{A} = k\sqrt{t} \tag{1}$$

$$k = \frac{Q}{A \cdot \sqrt{t}} \tag{2}$$

where Q is the water absorption at every time, A is the water absorption section area of specimen (40 mm × 40 mm), and t is the water absorption time (h).

2.3.2 Compressive strength test

The compressive strength was measured using a microcomputer controlled flexural and compression testing machine with the maximum loading of 300 kN at a loading rate of 0.6 kN/s. Noting that the treated side should be avoided during compressive strength test.

2.3.3 Mercury intrusion porosimetry (MIP)

Pore structure of the treated surface layer were characterised using mercury intrusion porosimetry (MIP) with AutoPore Iv 9510 (American Mike Pretic). The debris from the near surface of mortar's treated side (about less than 1 cm) were selected and tested.

2.3.4 X-ray Diffractometry (XRD)

After surface treatment, a layer of precipitated substance formed on the surface. For different surface treatments, the precipitated layer was scraped and grounded into the powder for XRD test. The near surface layer and interior substance from broken samples were collected to preserve in anhydrous ethanol, which could stop the future hydration. The preserved samples were picked up into an agate mortar to grind till the grinding powder without sense of granularity. During the grinding process, some obvious big sand particles were picked out and the grinding powder was retained in a drying oven for XRD and thermogravimetric analysis (TGA) tests. XRD test was conducted using X-ray Diffractometry (X' Pert Pro produced by RIGAKU) with copper target. The XRD pattern was obtained by continuous scan from 10° to 60° with a step size of 0.02° and scanning rate of 5°/min.

2.3.5 Thermogravimetric analysis (TGA)

TGA test was conducted using a Thermal Analysis equipment TGA2 (Mettler-Toledo, Switzerland). The temperature ranged from room temperature (~20 °C) to 1000 °C in nitrogen atmosphere, with heating rate of 10 °C/min.

2.3.6 Scanning electron microscope-energy dispersive X-ray spectroscopy (SEM-EDS)

After surface treatment, the treated surface and near surface layer of samples were selected and dried before a thin layer of gold spraying for SEM scanning. Mineralogical compositions of the precipitated material were characterised using Field Emission Scanning Electron Microscope (Zeiss SIGMA) together with energy dispersive spectrometer (Oxford UltimMax 40), with accelerating voltage of 5 kV, magnification 5× up to 100,000× and resolution of 1.0–2.0 nm.

3. Results and discussion

3.1. Capillary water absorption coefficient

The effects of different soaking time on the capillary water absorption of mortar specimens with different calcium sources are shown in Fig. 2a, b and c. It can be clearly seen from the figure that the capillary water absorption of all specimens was generally increased with the increasing soaking time. The increment was fast in the first 9 h and then gradually became slow. Compared to that of the reference sample M50, the surface treatment led to a significant drop in the capillary water absorption of mortar, regardless of the type of calcium resource. As seen in Fig. 2a, for surface treatment with calcium source of CC, at all soaking time, the sample M50A05 (BS/CS = 1:2) exhibited the lowest water absorption, while the highest value was obtained in the sample M50A20 (BS/CS = 2:1). However, the difference between the three treated samples was not obvious. In contrast to the CC treatment, under the CN treatment, M50B20 (BS/CS = 2:1) exhibited a lower water absorption, while both M50B05 and M50B10 showed a higher water absorption (Fig. 2b). Regarding to CA surface treatment, a different trend from that of CC treatment and CN treatment can be observed (Fig. 2c), where the lowest water absorption occurred for M50C10, while the absorption content of M50C05 and M50C20 was slightly reduced. Moreover, regardless the source of calcium, the absorption of all samples after surface treatment with MICP was significantly reduced, which can be ascribed to the formation of some calcium carbonates on the treated surface of mortar, filling in the surface pores and thus water ingress into the interior would be hindered, decreasing the capillary water absorption to some extent. According to the data in Fig. 2a, b and c, the curves of capillary water absorption amount vs. square root of time are shown in Fig. 2d, e and f, respectively. And the calculated capillary water absorption coefficients (hereinafter referred to as coefficients) of all samples are presented in Fig. 3.

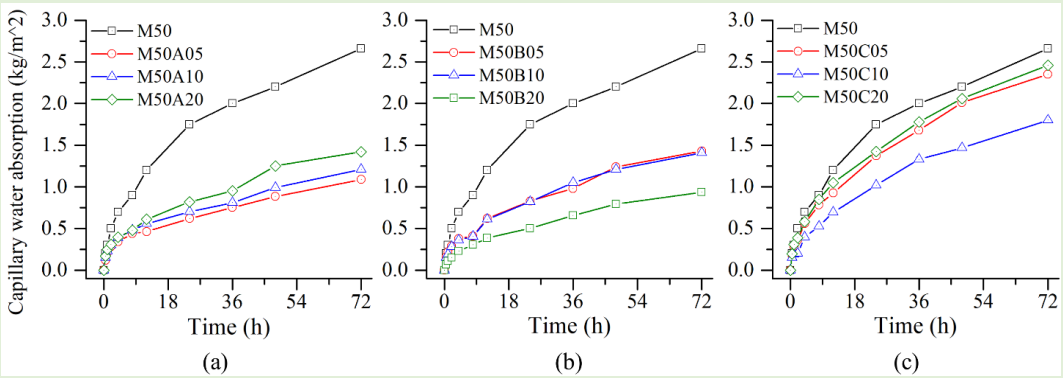

Fig. 2. Effect of different soaking time on the capillary water absorption of specimens with calcium source of (a) CC, (b) CN, and (c) CA.

From Fig. 3, the coefficients of all samples after surface treatment with MICP were lower than that of the reference sample M50, suggesting that surface treatment with MICP could reduce the coefficients of mortars. The average coefficients of treated samples with the calcium source of CC,

CN and CA were 0.15, 0.15 and 0.26 kg/(m2•h0.5), implying a 55%, 55% and 21% reduction compared to that of the reference sample M50 with the coefficient of 0.33 kg/(m2•h0.5), respectively. The specimens treated with the calcium sources of CC and CN presented a similar reduction in water absorbance coefficient, while those treated with the calcium source of CA indicated a much smaller reduction. For the same calcium source (e.g., CC), the coefficient increased with the increase of BS/CS ratio, while the coefficient of specimens with CN had no change when the BS/CS ratio went up from 1:2 to 1:1 but dropped when the ratio was further increased to 2:1. Differently, the coefficient reduced to the lowest when the ratio is 1:1 but then rose when the calcium source is CA. These imply that the change of coefficient with BS/CS ratio highly depended on the calcium source. For specimens treated with different calcium sources had different lowest coefficients.

The reduced coefficients of the treated samples can be ascribed to the change of the near surface layer and the precipitation layer on the surface [9]. During the surface treatment with MICP, a layer of $CaCO_3$ was generated on the surface of the treated samples [40]. The morphology and particle size of the generated $CaCO_3$, and its production on sample's surface would play important roles in the protection efficiency [26,41]. When the BS/CS ratio was 1:2, less bacteria was existed, and thus, less precipitation could be produced. For BS/CS ratio of 2:1, the supply of nutriment and calcium ion in the system were insufficient due to the lack of cementation solution, which led to a slow metabolism of bacteria and a less production of urease. The poor depositional environment resulted in a smaller deposition quantity of $CaCO_3$. The quantity of precipitated calcite was found to be the highest for the cases with CC, which could fill the surface pores to the maximum and improve the pore structure of the near surface layer, as well as the coefficients. At the same time, under the same BS/CS ratio of 1:1, specimens treated with different calcium sources showed the different lowest coefficients. Therefore, different calcium sources could also cause the difference of the production or morphology of $CaCO_3$.

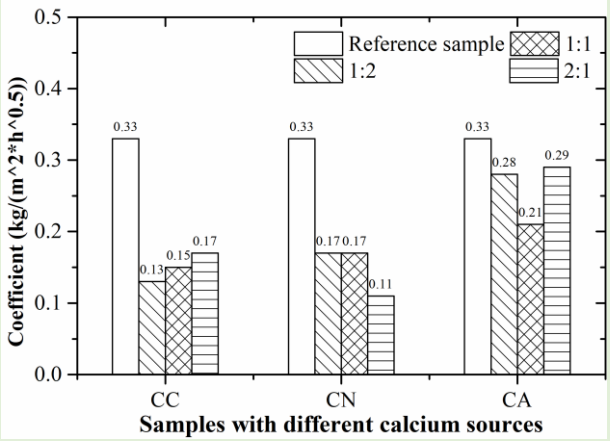

Fig. 3. Capillary water absorption coefficients of all samples.

3.2. Compressive strength

The compressive strength of all samples with and without surface treatment are presented in Fig. 4.

As shown in the figure, the compressive strength of the reference sample M50 was 43.2 MPa. It should be noted that MICP surface treatment changed in the compressive strength of mortar. Calcium source of CC provided a positive effect on the compressive strength of mortar, while CA offered a negative effect. When the calcium source in cementation solution was CC or CN, the compressive strength of the treated samples was about 4.18% and 2.67% higher than that of M50, respectively. If using CA as the calcium source, the compressive strength of mortar became lower than that of M50 with an average reduction of about 4.44%. All these suggest that the surface treatment with calcium source of CC and CN on mortar can induce an increase in compressive strength, while the surface treatment with calcium source of CA exhibited an adverse effect on the compressive strength of mortar. It should be noted that the strength increment or decrement of the treated sample was limited within 5%, suggesting that the surface treatment with MICP on mortar did not significantly affect the compressive strength of the specimen. Although the change in compressive strength depended on the calcium source used, for a specific calcium source, a similar trend can be observed for three solutions. Taking the calcium source of CC (M50A05, M50A10 and M50A20) as an example, the compressive strength of the treated sample was increased to the highest value when the BS/CS ratio rose from 1:2 to 1:1 but dropped when the ratio further increased to 2:1, implying that the BS/CS ratio of 1:1 can result in an improvement in compressive strength of mortar.

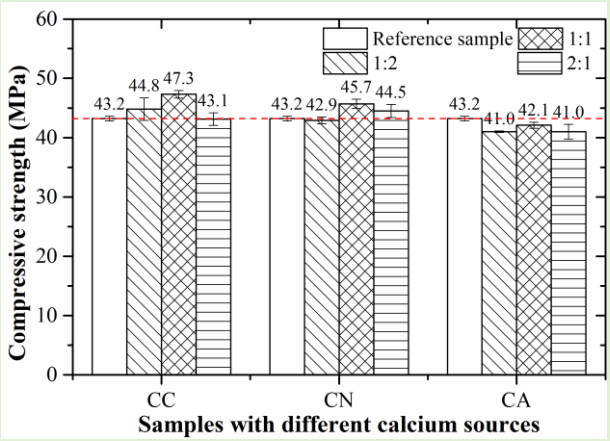

Fig. 4. Compressive strength of all samples with and without surface treatment.

The improved compressive strength of the treated samples can be ascribed to the enhanced pore structure of the near surface layer by MICP [42], while the local structure (surface structure) had only a slight influence on the compressive strength change of the treated samples [43,44]. When the calcium source in cementation solution was CA, compressive strength of treated samples was lower than the reference sample. Acetate is weak alkaline, while hydroxide and acetic acid are formed during the process of ionization. Acetic acid is weak acid, but it will erode the surface of mortar with acetic acid's local accumulation, which will increase the porosity of the surface, leading to a reduced compressive strength. In other conditions, calcium carbonate was generated on the surface or in the near surface layer of mortar, which would improve the pore structure of the local structure. In general,

the more calcium carbonate content, the more significant effect on the improvement in pore structure. When BS/CS ratio was 1:1, more calcium carbonate generated, which could fill in surface layer pores and improve the pore structure of the near surface layer, as well as the improvement of the compressive strength.

3.3. Pore structure

The cumulative and differential distribution of pore volume of the near surface layer of mortar specimens with the BS/CS ratio of 1:1 and the different calcium sources are presented in Fig. 5. Obviously, the cumulative pore volume of the samples after surface treatment with MICP were lower than that of the reference sample (M50) and the most probable pore size was decreased. To make it clearer, the details about the pore structure (pore volume distribution, pore volume fraction distribution and porosity) are summarized in Fig. 6. As shown in Fig. 6a, the total pore volume of the samples after surface treatment with MICP decreased significantly. Meanwhile, pore volume of pore size (50–200 nm), the harmful pore for the strength [45], was decreased after surface treatment, and pore volume of pore size (< 20 nm), the harmless pore for the strength, was increased. Similarly, as shown in Fig. 6b, pore volume fraction of harmless pore significantly increased after surface treatment, while pore volume fraction of harmful pore was decreased. These results indicated that that after surface treatment, part of the harmful pores was transformed to harmless pores, which decreased the pore size and made pore structure more density. Fig. 6c shows the porosity and pore size characteristics of all samples. Obviously, after surface treatment, porosity of all treated samples was reduced, and average pore size and median pore sizes were decreased as well.

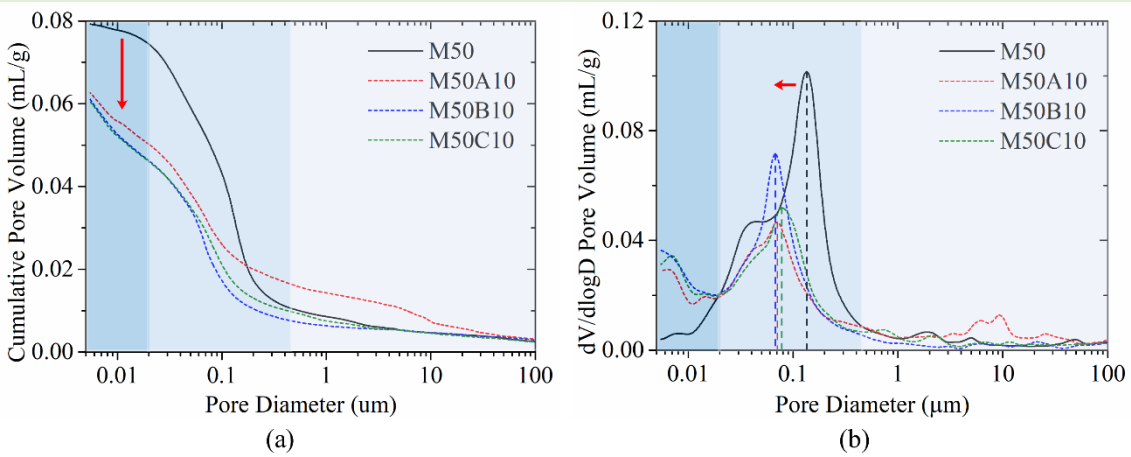

Fig. 5. (a) Cumulative distribution and (b) differential distribution of pore volume of samples.

It should be noted that the pore volumes of harmless pores and less harmful pores (pore size <50 nm) of treated samples M50A10, M50B10 and M50C10 were about 0.024, 0.027 and 0.025 mL/g, respectively, which were about 20%, 31% and 25% higher than the reference sample M50. During the surface treatment, some bacterial solution and cementation solution might permeate into samples and generate some calcium carbonate to fill or clog the pores, which would fine the pore structure and reduce its porosity [46,47]. The increase of pore volumes of harmless pores and less harmful

pores would make the interior pores smaller, which is beneficial to pore structure and improve the compressive strength.

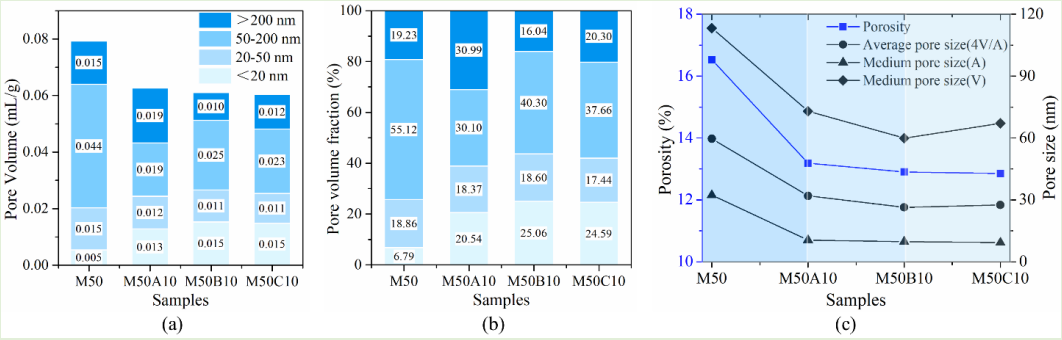

Fig. 6. Pore structure of all samples in terms of (a) pore volume distribution, (b) pore volume fraction distribution, and (c) porosity.

3.4. XRD analysis

The XRD spectra for the precipitated layer on the surface of the samples are shown in Fig. 7. As shown in the figure, the most identical diffraction peaks were corresponding to the peaks of calcite (PDF. No: 01-086-0174) and vaterite (PDF. No: 01-072-0506), which indicated that the generated substance on mortar's surface by MICP was the mixture of calcite and vaterite. It should be noted that the substance depended on the type of calcium source. For example, when the CC (sample M50A20) and CN (sample M50B20) was applied, the diffraction peak intensity of calcite was much higher than that of vaterite, suggesting that the main substance was calcite. However, for the sample treated by CA (sample M50C20), the diffraction peak intensity of calcite is the same as that of vaterite, indicating that the main substance is the mixture of calcite and vaterite.

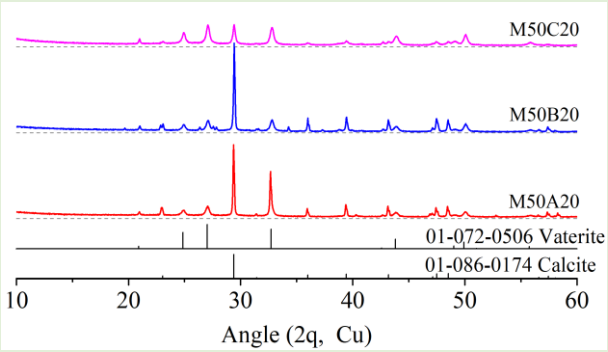

Fig. 7. X-ray spectra of the generated layer of the surface.

To identify the difference between the matrix and surface layer, the mineral compositions of the matrix and near surface substance were charactered by XRD and the X-ray spectra are shown in Fig. 8. As shown in Fig. 8a, c and e, the main crystals of interior substance of all samples were silica and portlandite (CH), accompanying with some dolomite exists. It should be noted that the content of silica was the highest and its diffraction peak was extremely high, which could be due to that the silica mainly might come from the silica sand in mortar. Comparing to the reference sample M50, the CH diffraction peak intensity of surface treated samples was a little higher. The reason might be due

to the further hydration of the mortar during the surface treatment, which resulted more content of hydrated CH. Comparing with the three different calcium sources, the diffraction peak intensity differences within those three samples (such as M50A05, M50B05 and M50C05 in Fig. 8a, or M50A10, M50B10 and M50C10 in Fig. 8b, or M50A20, M50B20 and M50C20 in Fig. 8c) were not obvious. Therefore, it can be safely deducted that the different surface treatments have no influence on the hydration products of the matrix.

Fig. 8b, d and f present that the main crystals of the near surface layer are silica and CH, it also contains some dolomite and calcite. Comparing to the reference sample M50, almost all treated samples' CH diffraction peaks reduced, and calcite diffraction peaks increased slightly. The reasons caused this change were (1) during the surface treatment process, bacterial solution permeated into the surface layer, which could decrease pH value of the pore solution and cause the decomposition of CH, (2) the decomposition of CH could release some Ca2+, which would be consumed to form calcite, (3) the MICP action on the surface of treated samples generated a lay of calcium carbonate, which strengthen calcite diffraction peak. Comparing to the hydration products of the interior substance, for the materials from near surface layer, the intensity of calcite increased and that of CH decreased, which was the same to the above.

It should be noted that when the different calcium source was applied, the intensity of CH diffraction peak and calcite diffraction peak were different, too. As shown in Fig. 8b, d and f, when the calcium source was CN (for example, sample M50B05, M50B10 and M50B20), the intensity of the diffraction peak of calcite was the lowest and the diffraction peak of CH was the highest. It may be resulted to the inhibition effect of urease activity by NO_3^- [48], which would reduce the precipitation of calcite. Meantime, the particle size of generated calcium carbonate was small in the presence of NO3−, which could fill pores in surface layer better and prevent the ingress of bacterial solution. Therefore, the consumption of CH was small, and the average capillary water absorption coefficient was lower. When the calcium source was changed to CC or CA, the height of diffraction peak of calcite was higher and that of CH was lower comparing to samples with the calcium source of CN. The filling effect from the generated calcium carbonate was poorer than that with calcium source of CN, which therefore, more bacterial solution could ingress into the surface layer and more CH was consumed to form new reaction hydrates, densifying the structure of surface layer. However, since the acetate is weak alkaline, hydroxide and acetic acid are formed during the process of ionization. Although the acetic acid is weak acid, it can erode the surface of mortar at the place where the acetic acid's local accumulation. Therefore, even though the calcium carbonate content on the surface of the treated material is high, local accumulation of acetic acid may lead to local erosion, so the CH content is reduced and the capillary water absorption coefficient on the surface was increased.

With the increase of the BS/CS ratio, such as samples from M50C05, M50C10 to M50C20, the

intensity of diffraction peak of calcite increased first and then reduced, while that of CH reduced. When the BS/CS ratio was 1:1, the intensity of the diffraction peak of calcite was the strongest, which indicated that the precipitated calcite was found to be the highest for this case. Calcite content of near surface layer played an important role in pore structure. The decrease of CH content was caused by the content of bacterial solution. The pH value of stable bacterial solution was about 9.5, which was lower than that of pore solution in mortar surface layer with pH value of ~12.5. When more bacterial solution was added in the surface, more CH would be decomposed to supply the basicity for pore solution. Therefore, CH content was less. The combination of reaction products CH and calcite filled in the surface layer pores and optimize the pore structure of the mortar's surface layer.

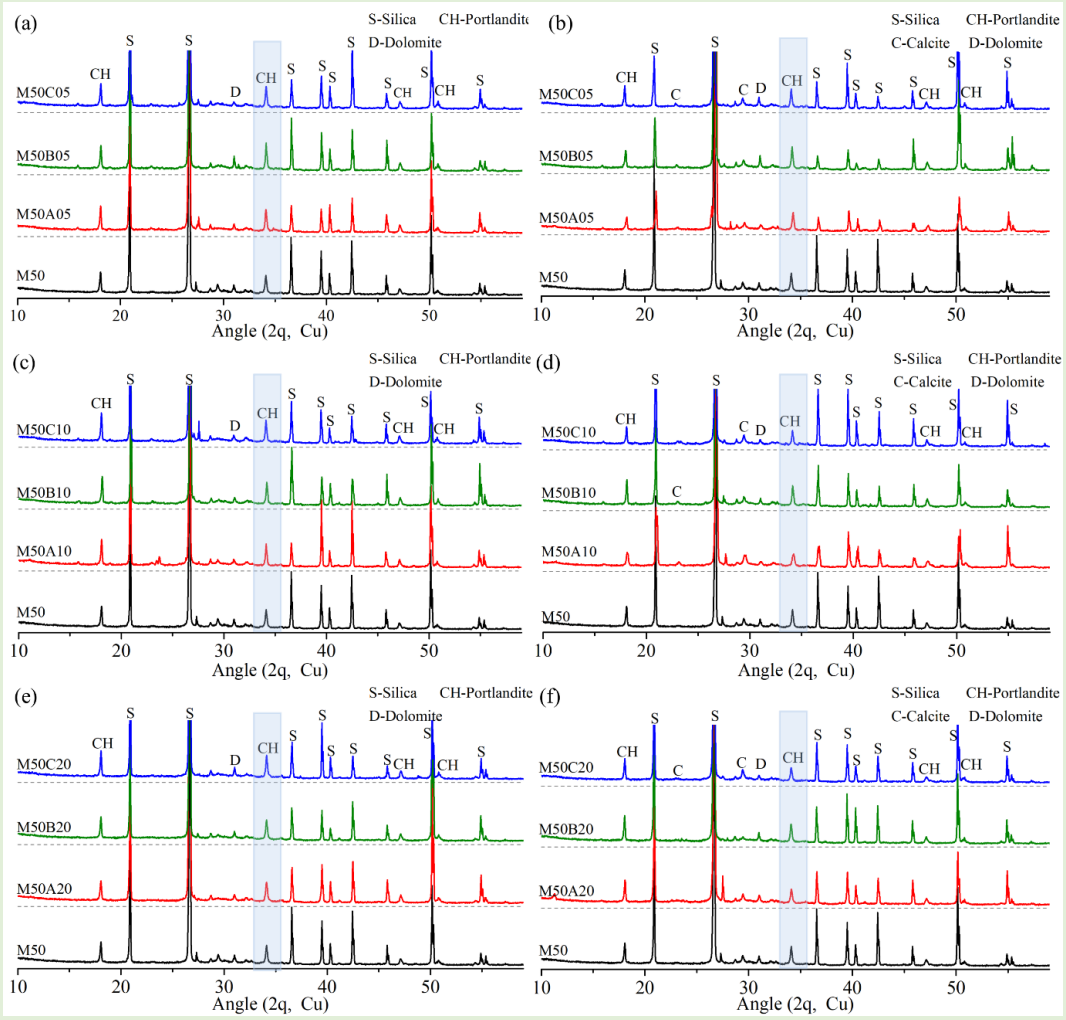

Fig. 8. X-ray spectra of the interior (a) (c) (e) and surface layer (b) (d) (f) of all samples.

3.5. TGA analysis

The TG-DTA curves of both interior substance and surface layer of samples prepared under the BS to CS ratio of 1:1 are shown in Fig. 9. Three endothermic peaks were identified in DTA curves: (1) at the temperature before 200 °C, which represents the loss of free and crystalline water of hydration products; (2) between 400 and 500 °C, which represents the decomposition of CH, which will convert to CaO and H_2O; (3) between 500 and 700 °C represents the decomposition of calcite, which will convert to CaO and CO_2. The difference of all samples at each endothermic peaks were not obvious,

except for the endothermic peak at the temperature between 500 and 700 °C of the surface layer as shown in Fig. 9b. All endothermic peaks at the temperature between 500 and 700 °C of the surface layer were higher than those of the interior substance, too. It can indicate that, comparing to the interior substance, more calcite was formed on the surface after surface treatment. It should be noted that different calcium source resulted different quantity of calcite, which is corresponding to the result of XRD.

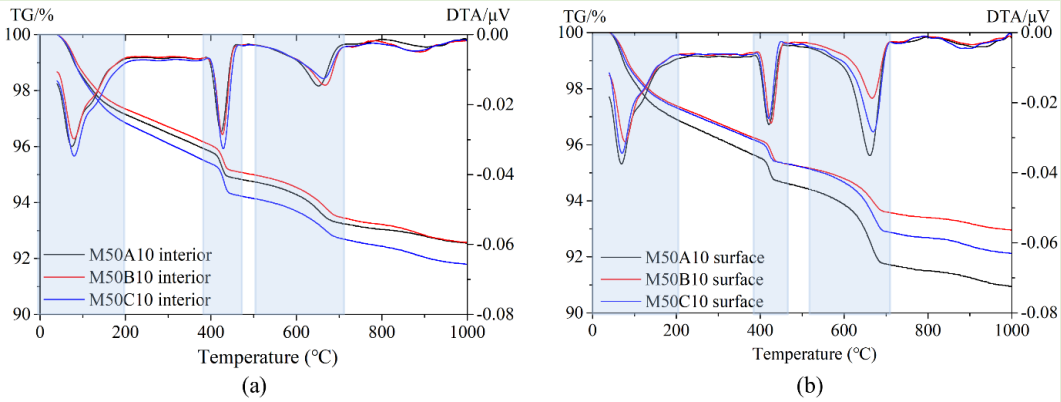

Fig. 9. TG-DTA curves of samples (a) interior (b) surface layer.

The weight loss of all samples at different temperature ranges were calculated from TG and DTA curves, and the results are shown in Fig. 10. In general, weight loss before 200 °C was the greatest, and the second was between 500 and 700 °C, the smallest weight loss happened between 400 and 500 °C. Compared to the reference sample M50 marked by the red dotted line, after surface treatment, the weight loss of surface layer and interior substance before 200 °C of almost all samples increased, suggesting that the total hydration products increased after surface treatment. The weight loss of surface layer between 400 and 500 °C of samples M50A05, M50A20, M50B05, M50B20 and M50C20 increased and other samples such as M50A10, M50B10, M50C05 and M50C10 decreased to some extent, while that of interior substance all increased. The weight loss of surface layer between 500 and 700 °C significantly increased, while that of interior substance of some treated samples such as M50A05, M50A20, M50B20 and M50C05 decreased.

Generally, after surface treatment, for the interior substance, the total hydration products, particularly for CH, was increased, while the content of calcite was decreased. For the near surface layer, the total hydration products increased with decreased CH content and increased calcite. After surface treatment by MICP, some bio calcium carbonate generated on the surface, which increased the content of calcite on the surface layer. The weight loss between 400 and 500 °C of the surface layer was lower than that of the interior substance expect for sample M50B20, indicating that the surface treatment with MICP reduced CH content of surface layer. The reasons could be attributed to that CH was acted as calcium source to form the calcite during the surface treatment process. For the same calcium source, with the increase of BS/CS ratio, CH content of the surface layer decreased first and then increased. CH content was the lowest with the BS/CS ratio of 1:1. For the same BS/CS

ratio, when calcium source was CN, average content of CH was the highest. The improvement of pore structure in near surface layer could play a good role of sample's strength. The lower of the CH content of the surface layer, the more influence of MICP on. It indicated that more CH was consumed during the process of MICP. On one hand, it can be acted as calcium source to form calcium carbonate; on the other hand, the decomposition of CH can influence the microstructure and increased macropore ratio of the near surface layer.

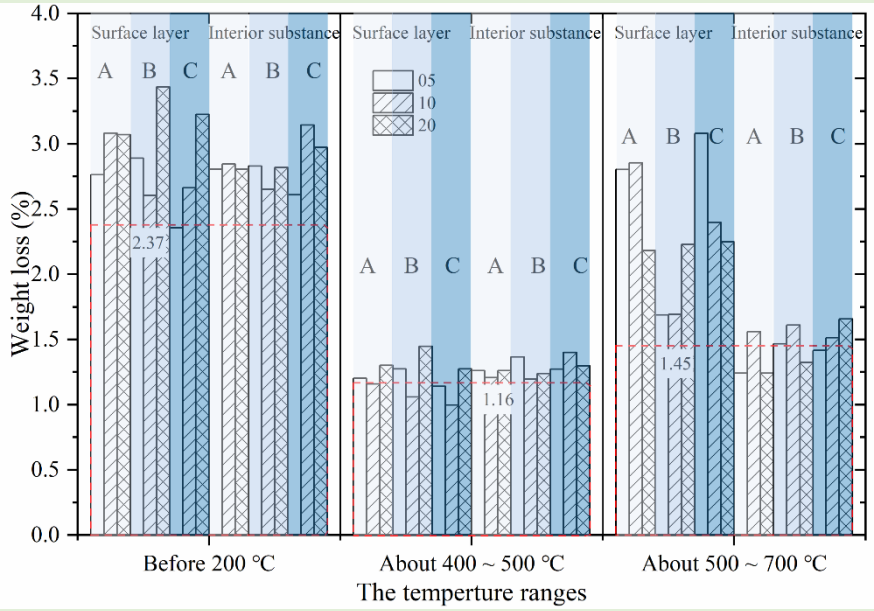

Fig. 10. Weight loss of surface layer and interior substance of all samples at different temperature ranges.

3.6. Microstructure

Fig. 11 illustrates the morphology of the surface layer and interior substance of the reference sample M50. As seen in Fig. 11a, the surface of M50 contained varying particle sizes, leading to a porous surface [49]. As marked with red circle in the figure, some hydration products such as C–S–H gel can be found through the pore. Fig. 11b indicates that the interior of M50 was mainly composed of cluster hydration product C–S–H gel with very dense growth. EDS results of C–S–H gel suggests that the main contents were O, Si, Ca, and few C, Al and Mg and the ratio of Ca/Si was about 0.97.

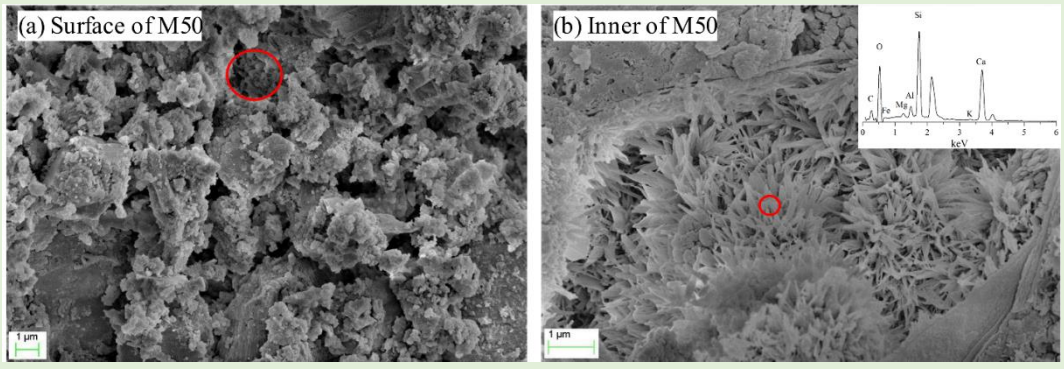

Fig. 11. SEM images of the reference sample M50.

After MICP surface treatment, the morphology of the surface and interior substance of each

sample is shown in Fig. 12. For example, on the surface of sample M50A05 (Fig. 12Fig. 12a1), many spherical, hexagonal-prismatic and platelike substances were observed, which covered on the porous surface of mortar and densified the porous structure on the surface. The surface of specimen M50A10 (Fig. 12b1) was covered by a large number of spherical substances, some of which are integrated with the surface of the specimen, and some of which are covered on the surface with complete morphology. A single sphere, or two spheres connected to each other can be found. Some spherical materials have smooth surfaces, and some have very rough surfaces that seem to consist of crystals growing at different angles. Size of the spherical substances are different, from 2 to 30 μm, spherical material overlapped with each other, fusion, forming a whole. In addition, the bacteria can be traced by the spherical substance. The surface of sample M50B05 (Fig. 12c1) was covered by a layer of spherical substance produced by deposition, which was similar to other MICP surface treated specimens. Due to the less bacterial solution during the surface treatment, there is not enough spherical substance produced to form a denser sedimentary layer [50]. According to EDS results, the main elements of large spherical substance deposited on the surface are Ca, C and O. Meanwhile, by magnifying the rough spheres, some smaller spheres at nanoscale can be observed, which were Ca, C and O. The surface of sample M50B10 (Fig. 12d1) was composed of a layer of spherical and fine granular substances, covering on the original mortar surface. Meanwhile, the magnification shows that the surface is composed of small particles, which can increase the density of the sediment layer. The surface of the whole is like a fish scale covering the surface of the specimen. The surface of sample M50C10 (Fig. 12e1) was consisted of spherical substances with different sizes. After magnification, it is found that the surface of spherical substance was composed of smaller particles.

Comparing to the reference M50, the surface treatment with MICP also exhibited the change on the morphology of the interior substance of cement mortar. For example, in the interior of sample M50A05 (Fig. 12a2), although the hydration products, such as needle and rod like substances, fibrous or tinfoil like C–S–H gel, was observed, the nanoscale spherical substances (marked in red circle) was also be observed filling around the hydration products. From the EDS result, it can be speculated that the nanoscale spherical substances were calcium carbonate, it could effectively fill the interior pores. Moreover, the interior of sample M50A10 (Fig. 12b2) was mainly composed of C–S–H gel clusters with some rod-like substances and spherical substances. It should be noted that the spherical material was sticked on rod and C–S–H surfaces. EDS results showed that the cluster C–S–H gel mainly was consisted of Ca, Si and O, with a small amount of Al and Mg, and its Ca/Si ratio was about 2.46. Compared with the original sample, its Ca content was relatively high, which may be caused by the addition of calcium source into the mortar. In sample M50B05 (Fig. 12c2), some coarse fibrous C–S–H gel and nanoscale spherical substances was observed. EDS results showed that the coarse fibrous C–S–H gel mainly was consisted of Ca, Si and O, it also contained a small amount of

Al and Mg, and its Ca/Si ratio was about 1.82. In the interior of sample M50B10 (Fig. 12d2), there are mainly some cluster-like C–S–H gels, needle-rod material and hexagonal platelike CH was observed. Moreover, some nanoscale spherical substances can be found on the surface of the needle-rod materials in the magnification picture. In sample M50C10 (Fig. 12e2), in addition to cluster-like C–S–H gel, needle-rod substance and hexagonal plate-like CH, there are still some nanoscale spherical substances produced. EDS results showed that the main elements of cluster C–S–H gel were Ca, Si, O, and a small amount of Al and Mg, and the Ca/Si ratio was about 2.31.

The improvement on the strength of treated samples could be attributed to the change of the near surface layer, including the evolution of pore structure and the change of reaction products. During the surface treatment, some bacterial solution and cementation solution permeated through the porous surface into the near surface layer, then some nanoscale $CaCO_3$ was generated, which could be attached to cement's hydration products to fine interior pore structure [17]. After surface treatment, cluster hydration product C–S–H gel converted to net and tinfoil like C–S–H gel, and the Ca/Si ratio increased from 0.97 to higher than 2. The increasing Ca/Si ratio was mainly due to the generated nanoscale $CaCO_3$ between gel pores, which improved the content of calcium. As shown in Fig. 12, large amount of nano-sized spherical CaCO3 was formed on the surface of hydration products, such as C–S–H gel and CH, which could fill in interior pores, especially gel pores among C–S–H gel [51, 52]. As shown in Fig. 12b1, d1 and e1, the spherical $CaCO_3$ were observed, which were integrated with the surface of the specimen, and covered on the surface with complete morphology. Just analysis from the surface morphology, the integrity of surface layer of sample M50A10 was the best (Fig. 12b1), while there were lots of different sizes' pores of surface layer of samples M50B10 and M50C10. As displayed in Fig. 6, pore volume of harmless pores and less harmful pores of sample M50B10 is the highest, which is beneficial to pore structure. The content of CH and calcite of surface layer of sample M50B10 was in the middle. The combination action of the best pore structure of near surface layer and the general precipitation layer on the surface made the lowest of the coefficient of sample M50B10. Therefore, pore structure of the near surface layer and the quantity of the precipitated layer have important role on the coefficients of samples. As seen in Fig. 12b2, the nanoscale calcium carbonate was generated on the surface of C–S–H gel. The nanoscale $CaCO_3$ content of sample M50A10 was the greatest, which could fill more pores and make the structure denser. Therefore, the compressive strength were improved.

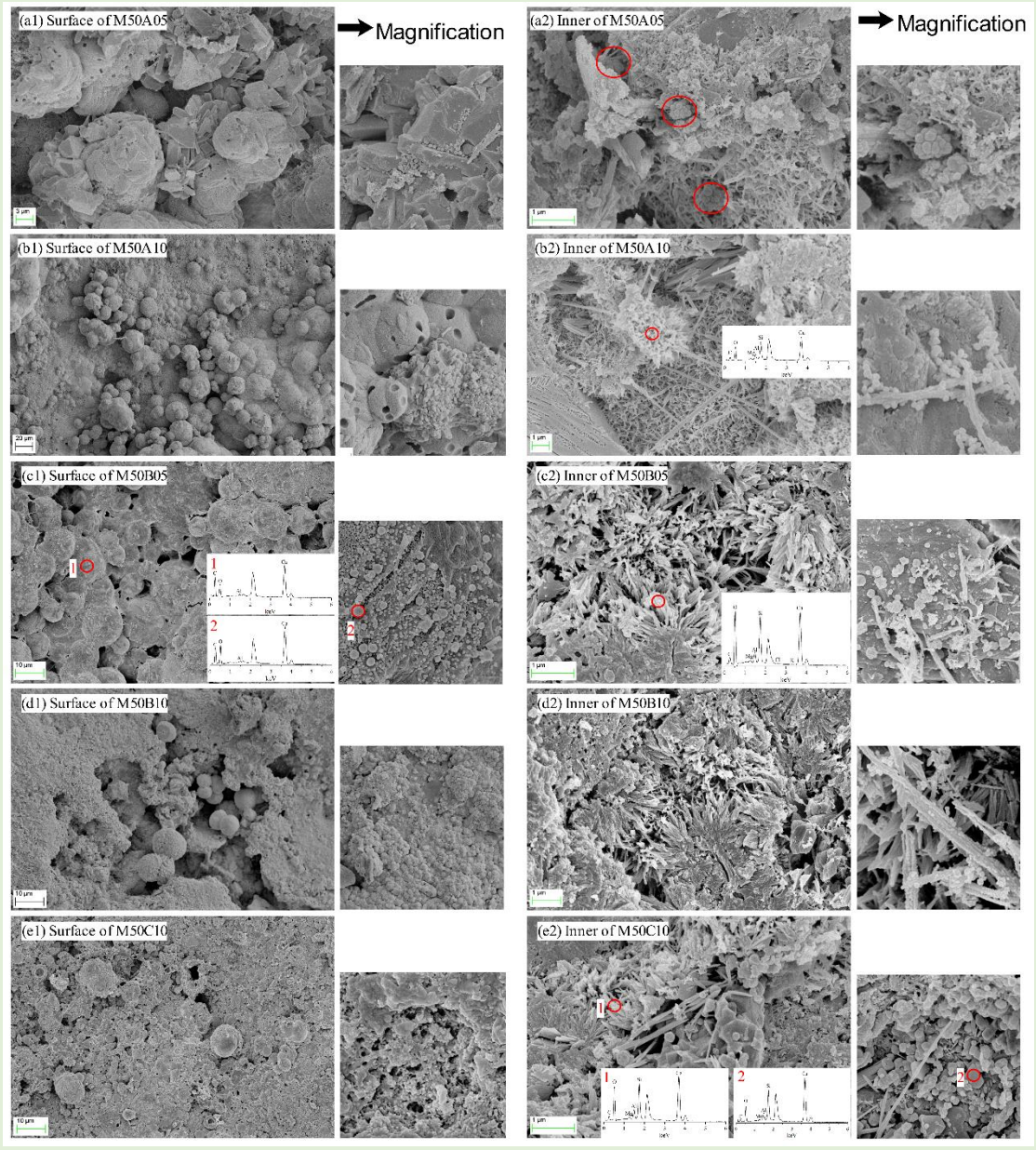

Fig. 12. SEM-EDS results of MICP surface treated samples.

4. Conclusions

To improve the effect of surface treatment with MICP in mortar, this paper presents an experimental study on capillary water absorption coefficient and compressive strength of the treated samples with consideration of the effects of bacterial solution to cementation solution volume ratios and different calcium sources in cementation solution, which is going to establish the relationship between microstructure and macro-property. Based on the experimental results obtained, the main conclusions can be drawn as follows:

(1) The surface treatment by MICP reduced the capillary water absorption coefficient significantly, while it affected the compressive strength of cement mortar slightly. Calcium sources (CC and CN), bacterial solution to cementation solution volume ratio (1:1) were beneficial to improve the compressive strength and reduce the coefficient.

(2) Surface treatment with MICP reduced the CH content and increased the calcite content of the near surface layer, while it showed limited influence on the hydration products of the interior substances. With the increase of BS/CS ratio, calcite content increased first, and then reduced. Calcium source especially CN is beneficial to the stability of CH, while it is adverse to the formation of calcite.

(3) Nanoscale calcite generated in the near surface layer from C–S–H gels and rod-like hydration product consumed CH and fill in gel pores, which increased the Ca/Si ratio of C–S–H, pore volume of harmless pores and decreased the average pore size.

(4) The improved compressive strength could be due to the refined pore structure of the near surface layer, the combination effect of improved pore structure of the near surface layer and the precipitation layer of MICP on the surface reduced the coefficients effectively.

Acknowledgments

The authors greatly acknowledge the financial support from the National Key R&D Program of China (Grant No. 2020YFC1806401), the Application Foundation Frontier Project of Wuhan City (Grant No. 2020010601012200) and the Visiting Researcher Fund Program of State Key Laboratory of Water Resources and Hydropower Engineering Science, China (Award No. 2019SGG01).

References

[1] L.V. Zhang, M.L. Nehdi, A.R. Suleiman, M.M. Allaf, M. Gan, A. Marani, et al., Crack self-healing in bio-green concrete. Compos B Eng, 227 (2021), p. 109397.

[2] Z.W. Jiang, L.J. Wang, Environment erosion and surface protection techniques of reinforced concrete, Corrosion Sci Protect Technol, 5 (2004), pp. 309-312.

[3] H.Y. Du, F.R. Qiu, C.J. Lin, Corrosion mechanism of concrete and new protection methods, Corrosion Sci Protect Technol, 3 (2001), pp. 156-161.

[4] Z. Suining, Q. Lin, H. Rui, W. Jiangtao, W. Zhenjun, Erosion damage and expansion evolution of interfacial transition zone in concrete under dry-wet cycles and sulfate erosion, Construct Build Mater (2021), p. 307.

[5] G. Liang, T. Liu, H. Li, K. Wu, Shrinkage mitigation, strength enhancement and microstructure improvement of alkali-activated slag/fly ash binders by ultrafine waste concrete powder, Compos B Eng, 231 (2022), p. 109570.

[6] C. Qian, J. Wang, R. Wang, L. Cheng, Corrosion protection of cement-based building materials by surface deposition of $CaCO_3$ by Bacillus pasteurii, Mater Sci Eng C, 29 (2009), pp. 1273-1280.

[7] X. Sun, L. Miao, L. Wu, H. Wang, Theoretical quantification for cracks repair based on microbially induced carbonate precipitation (MICP) method, Cement Concr Compos, 118 (2021), p. 103950.

[8] P. Termkhajornkit, T. Nawa, Y. Yamashiro, T. Saito, Self-healing ability of fly ash–cement systems, Cement Concr Compos, 31 (2009), pp. 195-203.

[9] L. Basheer, J. Kropp, D. Cleland, Assessment of the durability of concrete from its permeation properties: a review, Construct Build Mater, 15 (2001), pp. 93-103.

[10] A. Bashiri Rezaie, M. Liebscher, M. Ranjbarian, F. Simon, C. Zimmerer, A. Drechsler, et al., Enhancing the interfacial bonding between PE fibers and cementitious matrices through polydopamine surface modification, Compos B Eng, 217 (2021), p. 108817.

[11] C.B. Cheah, L.E. Tan, M. Ramli, The engineering properties and microstructure of sodium carbonate activated fly ash/slag blended mortars with silica fume, Compos B Eng, 160 (2019), pp. 558-572.

[12] W. De Muynck, K. Cox, N.D. Belie, W. Verstraete, Bacterial carbonate precipitation as an alternative surface treatment for concrete, Construct Build Mater, 22 (2008), pp. 875-885.

[13] A. Richardson, K. Coventry, J. Pasley, Bacterial crack sealing and surface finish application to concrete, Proceedings of fourth international conference on sustainable construction materials and technologies, Las Vegas, USA (2016).

[14] S. Liu, X. Gao, Evaluation of the anti-erosion characteristics of an MICP coating on the surface of tabia, J Mater Civ Eng, 10 (2020), p. 4020304.

[15] X. Pan, C. Shi, J. Zhang, L. Jia, L. Chong, Effect of inorganic surface treatment on surface hardness and carbonation of cement-based materials, Cement Concr Compos, 90 (2018), pp. 218-224.

[16] X. Wang, Z. Chen, W. Xu, X. Wang, Fluorescence labelling and self-healing microcapsules for detection and repair of surface microcracks in cement matrix, Compos B Eng, 184 (2020), p. 107744.

[17] W. De Muynck, D. Debrouwer, N. De Belie, W. Verstraete, Bacterial carbonate precipitation improves the durability of cementitious materials, Cement Concr Res, 38 (2008), pp. 1005-1014.

[18] J.W. Wang, Y.C. Ersan, N. Boon, N. De Belie, Application of microorganisms in concrete a

promising sustainable strategy to improve concrete durability, Appl Microbiol Biotechnol, 100 (2016), pp. 2993-3007.

[19] D.M. Iqbal, L.S. Wong, S.Y. Kong, Bio-Cementation in construction materials: a review, Materials, 14 (2021), p. 2175.

[20] S. Liu, R. Wang, J. Yu, X. Peng, Y. Cai, B. Tu, Effectiveness of the anti-erosion of an MICP coating on the surfaces of ancient clay roof tiles, Construct Build Mater, 243 (2020), p. 118202.

[21] B. Mu, Z. Gui, F. Lu, E. Petropoulos, Y. Yu, Microbial-induced carbonate precipitation improves physical and structural properties of Nanjing Ancient City Walls, Materials, 14 (2021), p. 5665.

[22] J. Dick, W. De Windt, B. De Graef, H. Saveyn, P. Van der Meeren, N. De Belie, et al., Bio-deposition of a calcium carbonate layer on degraded limestone by Bacillus species, Biodegradation, 17 (2006), pp. 357-367.

[23] W. De Muynck, K. Verbeken, N. De Belie, W. Verstraete, Influence of urea and calcium dosage on the effectiveness of bacterially induced carbonate precipitation on limestone, Ecol Eng, 36 (2010), pp. 99-111.

[24] W. De Muynck, S. Leuridan, D. Van Loo, K. Verbeken, V. Cnudde, N. De Belie, et al., Influence of pore structure on the effectiveness of a biogenic carbonate surface treatment for limestone conservation, Appl Environ Microbiol, 77 (2011), pp. 6808-6820.

[25] R. Alan, C. Kathryn, F.M. Alan, C. Jamison, Surface consolidation of natural stone materials using microbial induced calcite precipitation, Struct Surv (2014), pp. 265-278.

[26] N.W. Hudyma, R.W. Crowley, T.N. Ellis, Microbially induced calcite precipitation for the improvement of porous building stone, Proc ARMA (2018).

[27] W.K. Zhu, Fundamental studies of calcium carbonate mineralization induced by microbiologically in stone materials surface protection, Southwest University of Science and Technology (2008).

[28] J.M. Minto, Q. Tan, R.J. Lunn, G. El Mountassir, H. Guo, X. Cheng, Microbial mortar"-restoration of degraded marble structures with microbially induced carbonate precipitation, Construct Build Mater, 180 (2018), pp. 44-54.

[29] C. Feng, B. Cui, H. Ge, Y. Huang, W. Zhang, J. Zhu, Reinforcement of recycled aggregate by Microbial-Induced mineralization and deposition of calcium carbonate-influencing factors,

mechanism and effect of reinforcement, Crystals, 11 (2021), p. 887.

[30] N.N. Tri Huynh, N. Quynh Nhu, N. Khanh Son, Developing the solution of microbially induced $CaCO_3$ precipitation coating for cement concrete, IOP conference series, Mater Sci Eng, 431 (2018), p. 62006.

[31] P.B. Kulkarni, P.D. Nemade, M.P. Wagh, Healing of generated cracks in cement mortar using MICP, Civil Eng J, 6 (2020), pp. 679-692.

[32] S.A. Abo-El-Enein, A.H. Ali, F.N. Talkhan, H.A. Abdel-Gawwad, Utilization of microbial induced calcite precipitation for sand consolidation and mortar crack remediation, HBRC Journal, 8 (2019), pp. 185-192.

[33] J. Xu, X. Wang, Self-healing of concrete cracks by use of bacteria-containing low alkali cementitious material, Construct Build Mater, 167 (2018), pp. 1-14.

[34] J. Xu, X. Wang, A comparison investigation on the immersion and immobilization methods applied in the microbial surface treatment for concrete, Mater Rev, 32 (2018), pp. 4276-4280.

[35] J. Xu, X. Wang, W. Yao, Coupled effects of carbonation and bio-deposition in concrete surface treatment, Cement Concr Compos, 104 (2019), p. 103358.

[36] R.X. Wang, C.X. Qian, J.Y. Wang, L. Cheng, Different treated methods of microbiologically deposited CaCO3 layer on hardened cement paste surface, J Chin Ceram Soc, 36 (2008), pp. 1378-1384.

[37] R.X. Wang, C.X. Qian, Restoration of defects on the surface of cement-based materials by microbiologically precipitated $CaCO_3$, J Chin Ceram Soc, 36 (2008), pp. 457-464.

[38] L. Wang, S.H. Liu, Mechanism of sand cementation with an efficient method of microbial-induced calcite precipitation, Materials, 14 (2021), p. 5631.

[39] L. Wang, S.H. Liu, J. Ren, Effect of low-temperature treatment on bacterial cultivation in bacterial induced mineralization, Sci China Technol Sci 64 (2021).

[40] S. Choi, K. Wang, Z. Wen, J. Chu, Mortar crack repair using microbial induced calcite precipitation method, Cement Concr Compos, 83 (2017), pp. 209-221.

[41] R. Cardoso, R. Pedreira, S. Duarte, G. Monteiro, H. Borges, I. Flores-Colen, Biocementation as rehabilitation technique of porous materials, Springer Singapore, Singapore (2016), pp. 99-120.

[42] L. Skevi, B.J. Reeksting, T.D. Hoffmann, S. Gebhard, K. Paine, Incorporation of bacteria in

concrete: the case against MICP as a means for strength improvement, Cement Concr Compos, 120 (2021), p. 104056.

[43] Z.B. Bundur, A. Amiri, Y.C. Ersan, N. Boon, N. De Belie, Impact of air entraining admixtures on biogenic calcium carbonate precipitation and bacterial viability, Cement Concr Res, 98 (2017), pp. 44-49.

[44] Y. Zhao, L. Peng, W. Zeng, C.S. Poon, Z. Lu, Improvement in properties of concrete with modified RCA by microbial induced carbonate precipitation, Cement Concr Compos, 124 (2021), p. 104251.

[45] Z.W. Wu, H.Z. Lian, High performance concrete, China Railway Pubilshing House, Beijing (1999).

[46] T. Hoang, N.T. Dung, C. Unluer, J. Chu, Use of microbial carbonation process to enable self-carbonation of reactive MgO cement mixes, Cement Concr Res, 143 (2021), p. 106391.

[47] V. Whiffin, Microbial $CaCO_3$ Precipitation for the production of biocement, Murdoch University, Perth, Australia (2004).

[48] E.M. Do Nascimento, D. Eiras, L.A. Pessan, Effect of thermal treatment on impact resistance and mechanical properties of polypropylene/calcium carbonate nanocomposites, Compos B Eng, 91 (2016), pp. 228-234.

[49] S. Ruan, J. Qiu, Y. Weng, Y. Yang, E. Yang, J. Chu, et al., The use of microbial induced carbonate precipitation in healing cracks within reactive magnesia cement-based blends, Cement Concr Res, 115 (2019), pp. 176-188.

[50] D. Proudfoot, L. Brooks, C.H. Gammons, E. Barth, D. Bless, R.M. Nagisetty, et al., Investigating the potential for microbially induced carbonate precipitation to treat mine waste, J Hazard Mater, 424 (2022), p. 127490.

[51] M. Cao, X. Ming, H. Yin, L. Li, Influence of high temperature on strength, ultrasonic velocity and mass loss of calcium carbonate whisker reinforced cement paste, Compos B Eng, 163 (2019), pp. 438-446.

[52] Q. Fang, B. Song, T. Tee, L.T. Sin, D. Hui, S. Bee, Investigation of dynamic characteristics of nano-size calcium carbonate added in natural rubber vulcanizate, Compos B Eng, 60 (2014), pp. 561-567.